Optical Engineering

SPIEDigitalLibrary.org/oe

Uniaxial three-dimensional shape measurement with projector defocusing

Ying Xu
Song Zhang

Optical Engineering 51(2), 023604 (February 2012)

Uniaxial three-dimensional shape measurement with projector defocusing

Ying Xu
Song Zhang
Iowa State University Ames
Department of Mechanical Engineering
Ames Iowa, 50011

Abstract. Our study shows that the phase error caused by improperly defocused binary structured patterns correlates to the depth z. This finding leads to a novel uniaxial three-dimensional shape measurement technique without triangulation. Since the measurement can be performed from the same viewing angle, this proposed method overcomes some limitations of the triangulation-based techniques, such as the problem of measuring deep holes. Our study explains the principle of the technique and presents some experimental results to verify its feasibility. [DOI: 10.1117/1.OE.51.2.023604]

Subject terms: uniaxial; binary defocusing; three dimensional; fringe analysis; phase error.

Paper 111308P received Oct. 20, 2011; revised manuscript received Dec. 16, 2011; accepted for publication Dec. 21, 2011; published online Mar. 9, 2012.

1 Introduction

Due to their speed and flexibility, three-dimensional shape measurement based on digital sinusoidal fringe projection techniques have been playing an increasingly important role in optical metrology, and have been applied as a means of solving problems for numerous areas.[1] However, almost all these techniques require formation of a triangle for depth recovery. In other words, there must be a certain angle between the projection line and the imaging line in order to obtain the depth information for that point. However, for any triangulation-based three-dimensional shape measurement techniques, the occlusion of the system will be a problem. That is, the depth of a point cannot be recovered if just one of the two devices (camera or projector) can see it. Therefore, it is very difficult for a triangulation-based method to measure a small and deep hole, and difficult to recover depth for the occlusion area of the camera or the shadow area of the projector.

In contrast, if the depth information can be obtained without triangulation, the limitation of the a triangulation-based method can be significantly alleviated. The technique that does not require the projector and the camera to form a triangle is called uniaxial three-dimensional shape measurement.

There are a few optical techniques that can recover depth without triangulation. For instance, the shape from focus[2] and the shape from defocus[3,4] techniques measure depth by capturing a set of images with varying focal lengths. However, it is difficult for this technique to achieve high measurement accuracy because it is extremely difficult to precisely know the needed optical parameters (e.g., focal length), especially when the object does not have strong texture variations. Time-of-flight[5] technique retrieves depth by measuring the light traveling time from the point at which it leaves the sensor to that of its return. This technique can achieve higher speed and good quality measurement for long-range scenes, but cannot achieve high accuracy for short-range scenes.

0091-3286/2012/$25.00 © 2012 SPIE

Since the contrast of the fringe will change at different amounts of defocusing, Otani et al. presented a uniaxial three-dimensional shape measurement technique by analyzing fringe contrast (or data modulation).[6] This technology works well for uniform reflectivity surface, but has limitations when measuring high-contrast three-dimensional objects. Recently, Birch et al.[7] proposed a method to alleviate this problem by measuring the same surface another time with a different degree of defocusing. However, this technique slows down the measurement speed since it measures the object twice, and it is practically difficult to calibrate since it is usually not easy to precisely control the amounts of defocusing.

We propose a novel uniaxial three-dimensional shape measurement technique to alleviate the aforementioned problems through phase error analysis. Instead of analyzing the image itself, this technique obtains depth from the phase, which is inherently less sensitive to the optical properties of the surfaces to be measured. This new technique is based on the characteristics of the binary defocusing technique[8] that we proposed recently. In the study of the phase error caused by improperly defocused binary structured patterns, we found that the phase error can be described as a function of wrapped phase, $\phi(x, y)$, and the depth, z.[9] This finding provides an opportunity to determine the depth from the phase error, which inspires the development of this novel three-dimensional shape measurement technique. Since it is not necessary to form a triangle to determine the phase error caused by defocusing, this technique can also be used for uniaxial three-dimensional shape measurement.

Section 2 explains the principle of the proposed technique. Section 3 shows some preliminary experimental results to verify the feasibility of the proposed technique. Section 4 discusses the merits and possible limitations of the proposed technique, and finally Sec. 5 summarizes this paper.

2 Principle

2.1 *Three-Step Phase-Shifting Technique*

Phase-shifting methods are widely used in optical metrology because of their high measurement speed and high

achievable accuracy.[10] A three-step phase-shifting algorithm with a phase shift of $2\pi/3$ can be described as:

$$I_1(x,y) = I'(x,y) + I''(x,y)\cos[\phi(x,y) - 2\pi/3], \quad (1)$$

$$I_2(x,y) = I'(x,y) + I''(x,y)\cos[\phi(x,y)], \quad (2)$$

$$I_3(x,y) = I'(x,y) + I''(x,y)\cos[\phi(x,y) + 2\pi/3], \quad (3)$$

where $I'(x,y)$ is the average intensity, $I''(x,y)$ the intensity modulation, and $\phi(x,y)$ the phase to be solved for. From these three equations, the phase can be calculated by

$$\phi(x,y) = \tan^{-1}[\sqrt{3}(I_1 - I_3)/(2I_2 - I_1 - I_3)]. \quad (4)$$

This equation provides the wrapped phase ranging from $-\pi$ to $+\pi$ with 2π discontinuities.

2.2 *Binary Defocusing Technique*

Our recent study showed that by properly defocusing a binary structured pattern, a pseudo-sinusoidal one can be generated,[8] which is similar to the Ronchi grating defocusing method proposed by Su et al.[11] However, it is difficult for a Ronchi grating method to generate precise phase shift due to the requirement of mechanical adjustments. Therefore, the measurement error could be dominated by the phase shift error. In contrast, the phase-shift error of a digital fringe projection technique can be eliminated because of its digital fringe generation nature. Therefore, for a digital fringe projection system with the binary defocusing technique, the single dominant error source is the nonsinusoidal structure of the defocused binary patterns when the projector is not properly defocused; this magnitude of phase error correlates to the amount of defocusing, which will be addressed next.

2.3 *Phase Error Determination*

As explained earlier, if the projector is not properly defocused, the binary defocusing technique will result in significant phase error. For a conventional fringe projection system, the phase error is regarded as noise and needs to be reduced. Toward reducing the phase error caused by improper defocusing, we found that the phase error can be described as a function of wrapped phase, $\phi(x,y)$, and the depth, z.[9] This finding provides an opportunity to determine the depth from the phase error, which inspires the development of this novel three-dimensional shape measurement technique. Interestingly, the phase error becomes signal for this technique.

It is important to notice that it is very difficult to determine the phase error directly from three binary defocused fringe images because (1) the geometric shape of object may distort the fringe stripes; and (2) the camera and/or the projector lens may cause image distortion. Instead, we capture three ideal sinusoidal fringe patterns with exactly the same fringe pitch (number of pixels per fringe period). The phase error is determined by taking the difference between the phase, $\phi^b(x,y)$, obtained from the binary defocused patterns and the phase, $\phi^s(x,y)$, calculated from the ideal sinusoidal patterns,

$$\Delta\phi(x,y) = \phi^b(x,y) - \phi^s(x,y) \qquad \mod 2\pi. \quad (5)$$

Though the phase error can be calculated from the wrapped phase point by point, it practically uses the 2π modulus operation to account for the one-pixel shift due to camera sampling.

Let us take a look at the phase errors determined from Eq. (5) under different amount of defocusing. The first row of Fig. 1 shows the defocused binary patterns under different amounts of defocusing, while the second row of Fig. 1 shows the corresponding phase errors for three phase-shifted fringe patterns. It clearly shows (as expected) that when the projector is in focus, we have clear binary structures of the image, and the phase error is the largest; when the fringe patterns become closer and closer to ideally sinusoidal, the magnitude of phase error reduces accordingly, but the phase error structure remains.

3 Experiments

The proposed method was tested under the a system illustrated in Fig. 2 The system includes a digital-light-processing (DLP) projector (Samsung SP-P310MEMX)

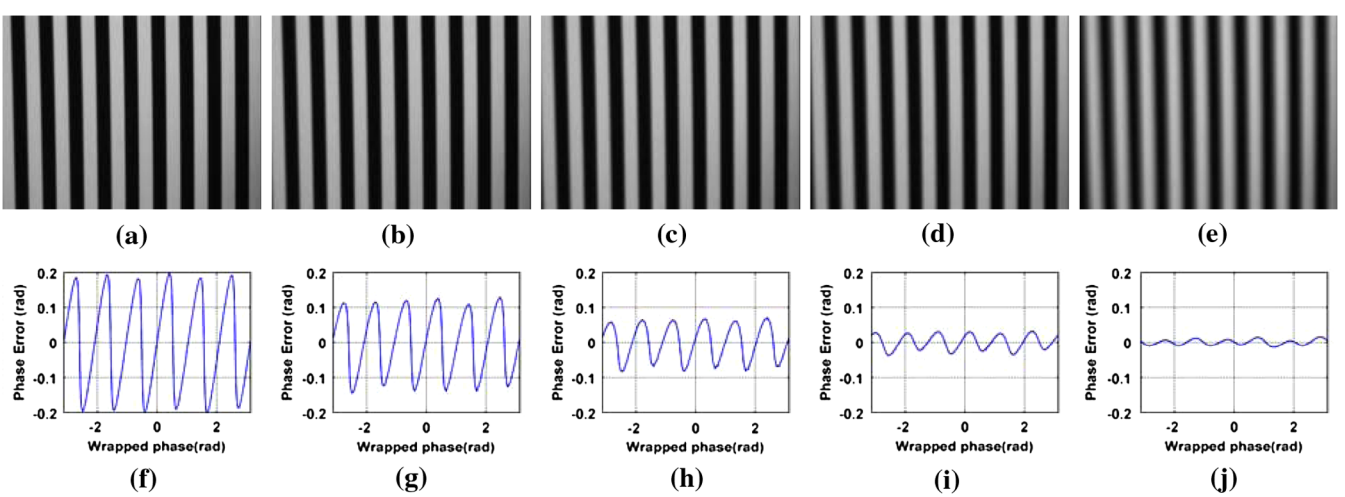

Fig. 1 Example of sinusoidal fringe generation by defocusing a binary structured pattern. The first row shows one of the three binary defocused patterns under each defocusing level. (a) shows the pattern when the projector is in focus; (b)–(e) show patterns when the projector is increasingly defocused; (f)–(j) show 240th row cross sections of the phase error maps.

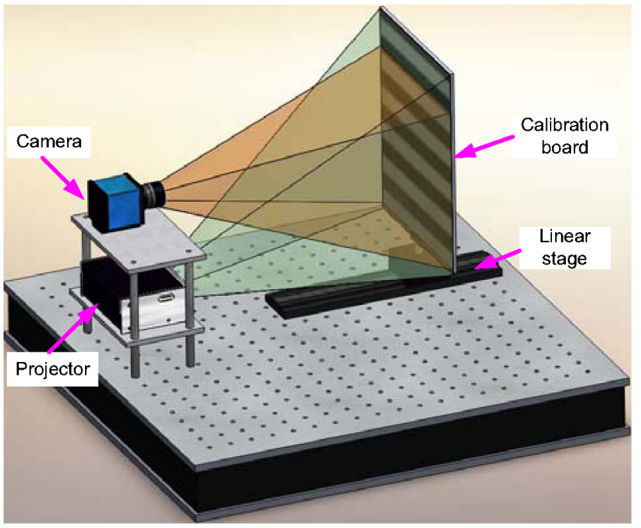

Fig. 2 System configuration.

and a digital charge-coupled detector (CCD) camera (Jai Pulnix TM-6740CL). The camera is attached with a 16-mm focal-length lens (Computar M1614-MP). The resolution of the camera is 640×480, with a maximum frame rate of 200 frames/sec. The projector has a resolution of 800×600 with a projection distance of 0.49 to 2.80 m. Figure 2 shows that the projector sits below the camera and projects horizontal stripes to make sure that the optical axis of the projector and that of the camera are approximately in parallel. It is practically difficult to configure the commercial video projector with the camera as a parallax system, and the current setup was found to be adequate to verify the proposed technique.

A linear translation stage was used to provide the desired motion backward and forward for calibration. In this research, we used the TECHSPEC Metric long travel linear translation stage. This stage is 250 mm long with a traveling accuracy of ± 0.05 mm. An uniform white flat object is mounted on top of the translation stage and travels with the stage for this study.

To calibrate the phase error function in terms of the wrapped phase, $\phi^b(x, y)$, and the depth (z), we set up the system in a manner so that the projected image is focused at a plane, and the camera is also focused at the same plane. This plane was chosen as $z = 0$; we then moved the plane toward the system with an increment of $\Delta z = 5$ mm. For each plane, we recorded three phase-shifted binary patterns, and three sinusoidal patterns with exactly the same fringe pitch, and computed the phase error using Eq. (5). In this research, the ideal sinusoidal fringe patterns were generated by correcting the nonlinear gamma of the projector using the technique presented in Ref. [12]. To reduce the random noise caused by the camera and the projector, each fringe pattern was an average of 15 patterns. Once the phase error is calculated, a 1024-element error look-up-table (LUT) was created by evenly quantize the wrapped phase within $[-\pi, +\pi]$ with a $2\pi/1024$ rad phase interval. Within each interval, the phase error is determined by averaging all points that fall within that interval.

For each plane, six fringe images are captured to determine the LUT. Figure 3 shows an example of how to create the LUT table. Figure 3(a) shows one of the three phase-shifted binary patterns, and Fig. 3(b) shows the wrapped phase from the binary patterns. At each position, three sinusoidal fringe patterns with the same fringe pitch were also captured, with one of them being shown in Fig. 3(c), and the resultant wrapped phase is shown in Fig. 3(d). Taking the difference of these two phase maps will result in the phase error illustrated in Fig. 3(e). However, because the phase error is higher frequency, it is difficult to see the error pattern without zooming in view. Figure 3(f) shows the 240th row cross section of the phase error map. It clearly shows periodical error structure while embracing randomness. The phase error is dependent of the camera sampling pixel position. In contrast, if we plot the phase error map as a function of wrapped phase, as shown in Fig. 3(g), it can be seen that the 6X frequency error structure

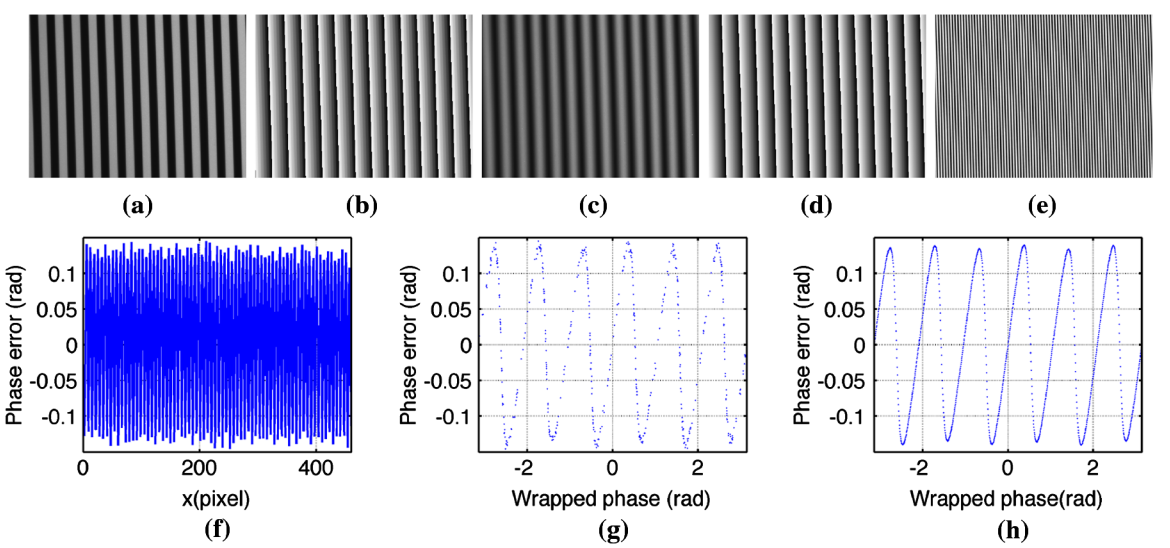

Fig. 3 Phase error determination. (a) One of the three phase-shifted binary structured patterns; (b) wrapped phase from the binary patterns; (c) one of the three phase-shifted sinusoidal fringe patterns; (d) wrapped phase from the sinusoidal patterns; (e) phase error map; (f) 240th row phase error against camera pixel; (g) the phase error against the wrapped phase $\phi(x, y)$; (h) 1024-element LUT.

is vivid, and is independent of sampling pixel position. Therefore, the phase error is described as a function of wrapped phase, and the LUT can be created. Figure 3(h) shows the 1024-element LUT created for this plane.

Our further experiments as shown in Fig. 4(a) indicated that the peak and valley points of the phase error occur at approximately $\phi(x,y) = \pm(2k+1)\pi/12$, $(k = 0, 1, \ldots, 5)$. For each of these points, the depth z can be approximated as a polynomial function of the phase error $\Delta\phi(x,y)$,

$$z_i = f(\Delta\phi_i; \phi_i). \tag{6}$$

Here $i = 1, 2, \ldots 12$. In the experiment, we used 28 planes to fit the polynomial functions. We found that the 3rd-order polynomials are sufficient to represent these functions. Figure 4(a) shows some of these LUT's. Furthermore, Fig. 4(b) shows the 562th element (one of the peaks) in each LUT along the depth z. This figure indicates that the peak phase error changes monotonically as a function of depth z, thus z can be obtained by solving the inverse function. Video 1 better visualizes the calibration LUTs with respect to the depth z. The red mark points on the video were plotted as Fig. 4(b).

Once the system is calibrated, we measured a step-height object with a known depth of approximately 53 mm. Figure 5(a) shows one of the binary fringe patterns, and Fig. 5(b) shows the phase error map. To better visualize the phase error difference on top and bottom surface, Fig. 5(c) shows the zoom-in view of the top surface, and Fig. 5(d) shows the zoom-in view of the bottom surface. It clearly shows the error magnitudes are quite different for different depth z.

The depth z can be determined for those peak and value points of the phase error map. Figure 6(a) shows the result that was smoothed by a 7×7 Gaussian filter. Our research found that the zero points of the phase error theoretically locates at $\phi(x,y) = \pm k\pi/6$, where $k = 0, 1, \ldots, 6$, in the wrapped phase domain. These zero points divide the wrapped phase evenly into 12 segments. Within each segment, the peak/valley points can be determined by finding the maximum/minimum phase errors. The plot was generated by re-meshing the none-grid sparse measurement points for the sake of visualization. Figure 6(b) shows one of the cross sections of the three-dimensional result. This preliminary data shows that the height of the three-dimensional object can indeed be successfully recovered from the phase error. However, one may notice that even after applying a Gaussian smoothing filter, the measurement accuracy is not very high; the reasons for this will be discussed in the next section.

4 Discussion

By analyzing the phase error, the depth information can be retrieved from the same view as the projection. This uniaxial three-dimensional shape measurement technique has the following merits:

- *Deep hole measurement*. This is an advantage of any uniaxial three-dimensional shape measurement technique, since it does not require formation of a triangle to recover depth.

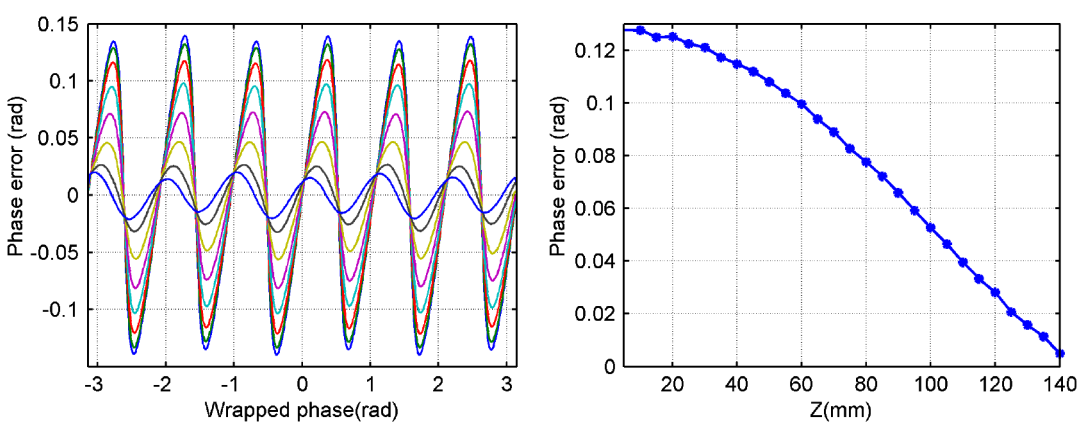

Fig. 4 The phase error changes with different depth z(Video 1). (a) Phase errors as a function of wrapped phase; (b) peak phase error shown in (a) as a function of depth z. (Video 1, MOV, 1.10 MB). [URL: http://dx.doi.org/10.1117/1.OE.51.2.023604.1]

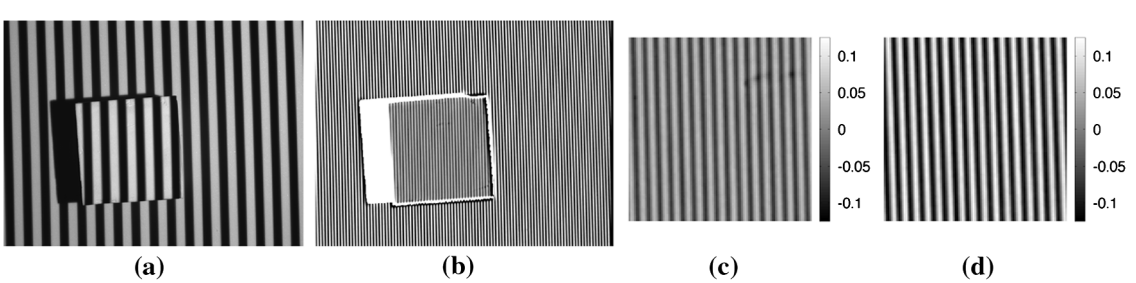

Fig. 5 Measurement result of a step-height object. (a) One of the binary fringe patterns; (b) phase error map; (c) zoom-in view of the top surface; (d) zoom-in view of the bottom surface.

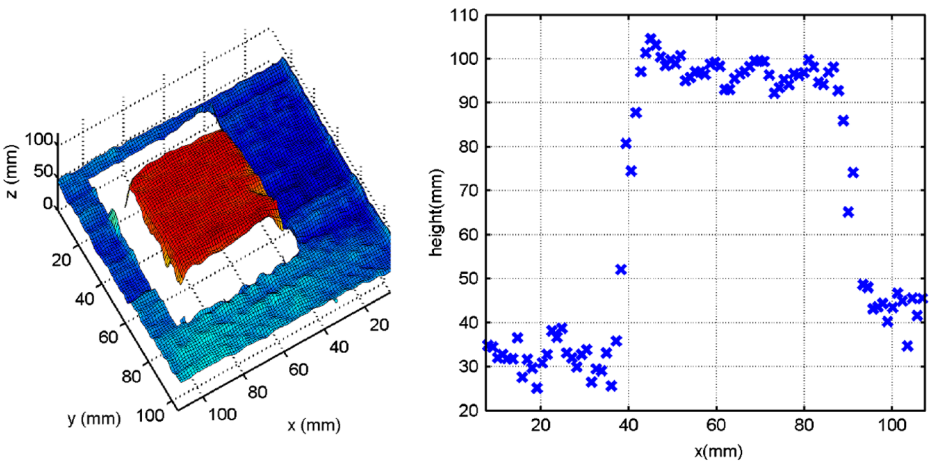

Fig. 6 Three-dimensional shape reconstruction of the step-height object shown in Fig. 5. (a) The three-dimensional plot; (b) one column cross section of the three-dimensional shape.

- *Potential high depth sensitivity.* Its depth sensitivity could be very high depending on the projection lens system used. If the depth of focus for the projector lens is very small, the amounts of defocusing will change rapidly with depth changes, and so will the phase error. Therefore, this measurement technique could be very sensitive to depth changes by properly selecting a lens system.
- *Less sensitivity to surface reflectivity variation*. Unlike the uniaxial method that retrieves depth by analyzing data modulation, this technique obtains depth from the phase, which is naturally less sensitive to surface reflectivity variations.
- *No phase unwrapping requirement*. Since the phase error is obtained by taking the difference of the phase obtained from the binary defocused patterns and that obtained from the ideal sinusoidal patterns, no phase unwrapping is necessary. Therefore, a single-wavelength phase-shifting algorithm can be used to measure an arbitrary step-height object.

However, despite its advantages, it has the following limitations:

- *Lower spatial resolution*. The current technique can only measure 12 points per period of fringe patterns, which is relatively low compared with some uniaxial three-dimensional shape measurement techniques that can achieve the camera-pixel spatial resolution.
- *Slower measurement speed*. This technique requires three phase-shifted sinusoidal patterns and three binary patterns to obtain one three-dimensional shape, and therefore its measurement speed is lower than that of a standard triangulation-based method that only needs three fringe patterns. In the meantime, for arbitrary step-height measurement when the absolute phase is required for a conventional triangulation-based fringe projection system, this technique might be faster since the conventional method practically requires more than six fringe patterns to obtain absolute phase point by point.
- *Better hardware requirement*. This technique requires precisely generated sinusoidal fringe patterns as a reference to obtain phase errors. Any error in the sinusoidal fringe patterns will be coupled into the final measurement. In addition, even for those peak points of the phase error, their actual values are relatively small (approximately ± 0.15 rad instead of $\pm\pi$ rad), making it more susceptible to noise than a conventional triangulation-based three-dimensional shape measurement system. Therefore, better hardware (both camera and projector) is needed to improve the measurement quality.
- *Divergent projection/capture*. Most commercially available video projectors use a divergent projection lens, which makes this proposed technique still feature the limitation of a triangulation-based method. To measure deep holes, the optical system has to be redesigned so that both the projector and the camera use collimated lenses.

5 Conclusions

This paper has presented a novel technique for uniaxial three-dimensional shape measurement by analyzing the phase error caused by improperly defocused binary structured patterns. The principle of this proposed technique has been explained, and preliminary experimental results have verified the feasibility of the proposed approach. However, the measurement quality is not very high at this stage. Our future work will focus on exploring methodologies to improve the spatial resolution, and to reduce the noise effect of this proposed uniaxial three-dimensional shape measurement technique.

References

1. G. Geng, "Structured-light 3D surface imaging: a tutorial," *Advances in Opt. and Photonics* **3**(2), 128–160 (2011).
2. S. K. Nayar and Y. Nakagawa, "Shape from focus," *IEEE T. Pattern Anal.* **16**(8), 824–831 (1994).
3. M. Subbarao, "Parallel depth recovery by changing camera parameters," in *2nd International Conference on Computer Vision*, 149–155 (1988).
4. M. Subbarao and G. Surya, "Depth from defocus: a spatial domain approach," *Int.J.Comput.Vis.* **13**(3), 271–294 (1994).
5. R. Lange and P. Seitz, "Solid-state time-of-flight range camera," *J. Quant. Elect.* **37**(3), 390–397 (2001).

6. Y. Otani et al., "Uni-axial measurement of three-dimensional surface profile by liquid crystal digital shifter," in *Proc. SPIE* **7790**, 77900A (2010).
7. P. Birch et al., "Depth from structured defocus that is independent of the object reflectivity function,"*Opt. Lett.* **36**, 2194–2196 (2011).
8. S. Lei and S. Zhang, "Flexible 3-D shape measurement using projector defocusing," *Opt. Lett.* **34**(20), 3080–3082 (2009).
9. Y. Xu et al., "Phase error compensation for 3-D shape measurement with projector defocusing," *Appl. Opt.* **50**(17), 2572–2581 (2011).
10. D. Malacara, Ed., *Optical Shop Testing*, John Wiley and Sons, New York, 3rd ed. (2007).
11. X.-Y. Su et al., "Automated phase-measuring profilometry using defocused projection of a ronchi grating," *Opt. Commun.* **94**(6), 561–573 (1992).
12. P. S. Huang, C. Zhang, and F.-P. Chiang, "High-speed 3-d shape measurement based on digital fringe projection," *Opt. Eng.* **42**, 163–168 (2003).

Ying Xu joined Iowa State University in 2008 to pursuit her BS in mechanical engineering. She is currently working with Dr. Zhang on structured-light three-dimensional optical metrology technologies. Her research interests include three-dimensional optical metrology, visualization, and image processing.

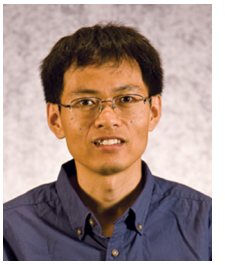

Song Zhang is an assistant professor of mechanical engineering at Iowa State University. He received his doctoral degree in mechanical engineering from Stony Brook University in 2005, and worked as a post-doctoral fellow at Harvard University from 2005 to 2008. His major research interests include superfast three-dimensional optical metrology, biophotonic imaging, three-dimensional machine and computer vision, human computer interaction, and virtual reality. He serves as a reviewer for over a dozen journals and is a member of SPIE.